The MMC Based DC Transformer With Reshaped Circulating Current

Wenlong Hou[1], Xiaodong Zhao[1], Binbin Li[1], and Dianguo Xu[1]

[1]School of Electrical Engineering, Harbin Institute of Technology, Harbin, China

Corresponding author: Binbin Li, libinbin@hit.edu.cn

Abstract

In this article, the modular multilevel converter based dc transformer (MMC-DCT) is proposed, which is constructed by modular multilevel arms, a transformer, and diode valves. Compared with other promising dc transformers, MMC-DCT can achieve high step-up ratio with MW level power transmission via intermediate medium-frequency transformer. The circulating current is reshaped into the trapezoidal wave instead of conventional dc wave, so that the capacitor voltage ripple can be suppressed significantly. Furthermore, by controlling three-phase currents of transformer into interleaved trapezoidal waves as well, smooth dc currents can be synthesized without bulky filters. The effectiveness is validated in simulation model and scaled-down laboratory prototype.

1 Introduction

With the increasing severe energy pressure, offshore wind power has been a major direction of renewable energy development due to steadier and stronger wind conditions than inland ones. In case of dc offshore wind farm, the dc transformer (DCT), the pivot for MVDC collection and HVDC transmission, remains several challenges, i.e., high voltage, large capacity, and high step-up ratio. To tackle the remaining hurdles, some academic scholars proposed MMC based DCTs relying on its flexible scalability and high voltage wave controllability. Reference [1] proposes a structure of dc-dc converter paralleling MMC three-phase output through bulky filters, where part of sub-modules (SMs) can be exploited at both MVDC and HVDC sides. Through injecting high amplitude of ac voltage and circulating currents into MMC, power can transfer between arms so as to realize the capacitor charge balancing. On this basis, reference[2] enables this toplogy bidirectional fault blocking capability similar to a dc circuit breaker by the utilization of cascaded full-bridge SMs. However, the shortage of this topology is additional heavy inductors (hundreds of millihenry) or active filters are indispensable. Reference [3] proposes a conventional MMC based front-to-front converter (MMC-FTF), using an intermediate-frequency transformer connected between two MMCs for electrical isolation. This topology can easily satisfy the requirement of high voltage and large capacity due to MMC. However, numerous components lead to an unrealistic solution for dc offshore wind farm with unidirectional power demand. To reduce the component count, reference [4] proposes a unidirectional DCT consisting of MMC at MVDC side and diode rectifier at HVDC side, since both the quantity and cost of diodes are much lower than SMs. Owing to the high controllability of MMC, the transformer currents are controlled into sinusoidal waves, which also leads to the large SM capacitor size. Therefore, reference [5] proposes a square-wave voltage modulated for high-frequency (1kHz) modular multilevel DCT, where the size of passive components such as arm inductors and SM capacitors can be reduced. However, the dc side current harmonics of this topology are serious. To tackle this difficulty, a hybrid-cascaded DC-DC converter applying the trapezoidal-wave current modulation is proposed in reference [6], where smooth dc currnts can be maintained without extra filters. Since the lack of intermediate transformer, power is transferred entirely by three-phase arms, resulting in large SM capacitor size. In [7], a novel DCT (TLC-MMC) is proposed, combining two-level converters in parallel at MVDC side and one MMC at HVDC side. But, the series connected IGCTs, employment of high insulation transformers and the large SM capacitor size would still be the concern.

This paper proposes the MMC based dc transformer (MMC-DCT) with reshaped circulating current strategy, which presents the advantages of high step-up ratio, high power, electrical isolation and smooth dc currents without any extra filters. Furthermore, owing to the reshaped circulating current, MMC-DCT can realize low capacitor voltage ripple and low switching loss compared to conventional dc wave.

2 Proposed MMC-DCT and Operation Principle

2.1 Circuit Configuration

As shown in Fig.1, the topology of MMC-DCT consists of three phase upper and lower arms (A_{pj} and A_{nj}) at MVDC side (j=a, b, c), one wye-wye connected 1:n three-phase transformer and one rectifier bridge constructed by six diode valves (D_1, D_3, D_5 and D_2, D_4, D_6) at HVDC side. Each arm is formed by N identical half-bridge SMs. L and L_k are the arm inductance and transformer leakage inductance, respectively. U_M, I_M are the voltage and current of MVDC side; U_H, I_H are the voltage and current of HVDC side; u_{pj}, u_{nj} and i_{pj}, i_{nj}

are the voltage and current of the upper and lower arm, respectively; i_j is the primary current of transformer.

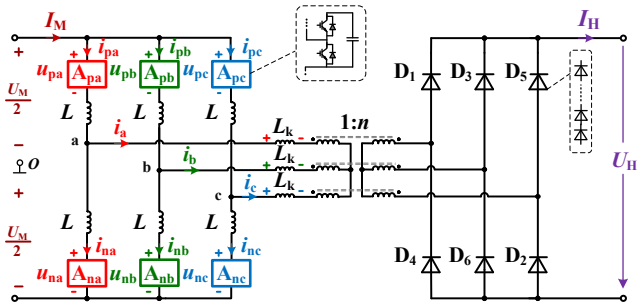

Fig. 1. Topology of the proposed MMC-DCT

2.2 Operation Principle

The operation waveforms of the proposed MMC-DCT are shown in Fig. 2. The arm voltage is designed as a two-level square wave, which assists in supporting the MVDC side voltage (U_M), as shown in Fig.2.(a) and (b). Both reshaped circulating currents shown in Fig.2.(c) and transformer currents shown in Fig.2.(d) are controlled into interleaved trapeziodal but identical waves, taking turns to carry currents at MVDC and HVDC sides, respectively. Meanwhile, the currents of upper and lower arm, shown in Fig.2.(e) and (f), exist a period of zero-current time (T_z) during each operation cycle (T_h), so that the switching loss can be reduced.

Applying Kirchhoff's law in Fig. 1, the basic circuit equations of voltage and current can be obtained:

$$\begin{cases} u_{oj}=\dfrac{U_M}{2}-u_{pj}-L\dfrac{di_{pj}}{dt} & i_{cj}=\dfrac{1}{2}(i_{pj}+i_{nj}) \\ u_{oj}=-\dfrac{U_M}{2}+u_{nj}+L\dfrac{di_{nj}}{dt} & i_j=i_{pj}-i_{nj} \end{cases} \quad (1)$$

where u_{oj} is the output voltage of phase j. Hence, based on Eq. (1), it is concluded that:

$$\begin{cases} U_M=2u_{comj}+2L\dfrac{di_{cj}}{dt} \\ u_{oj}=u_{diffj}-\dfrac{L}{2}\dfrac{di_j}{dt} \end{cases} \Rightarrow \begin{cases} u_{comj}=\dfrac{1}{2}(u_{nj}+u_{pj}) \\ u_{diffj}=\dfrac{1}{2}(u_{nj}-u_{pj}) \end{cases} \quad (2)$$

where u_{comj} and u_{diffj} are the common mode and differential mode components of arm voltage in phase j, respectively. It can be seen from Eq. (2) that u_{comj} controls the circulating current i_{cj} while u_{diffj} controls the transformer current i_j. Each operation cycle is composed of six holding stages (I~VI) as well as six holding stages (Ic~VIc). At the end of each holding stage, a commutation stage is followed, so as to avoid transformer saturation. The detailed analysis of operation stages is presented as follows.

Holding stage (III): The corresponding circuit is shown in Fig.2.(g), where phase a and phase c at MVDC side, D1 and D2 are in on-state. The MVDC current (I_M) is shared by two phases equally, which means $i_{ca}=i_{cc}=I_M/2$ and $i_{cb}=0$, respectively. Meanwhile, transformer currents of phase a and phase c are equal but opposite, i.e., $i_a=-i_c=nI_H$, whereas the current of phase b (i_b) remains zero. As a result, the SMs within phase b realize zero-current switching (ZCS) due to $i_{pb}=i_{nb}=0$. To get ready for the commutation stage, the voltage of A_{pb} (u_{pb}) gradually rises to $U_M/2+U_H/2n$, while the voltage of A_{nb} (u_{nb}) drops to $U_M/2-U_H/2n$. During above process, SMs are switched one by one to avoid spike current causing by excessive du/dt.

Commutation stage (IIIc): As shown in Fig.2.(h), the circulating currents commutate linearly between two phases, as do transformer currents. As for the former, by adjusting u_{coma} and u_{comb} to $U_M/2+U_{com}$ and $U_M/2-U_{com}$ respectively, arm inductors of phase a and phase b withstand opposite voltage U_{com}. Therefore, i_{ca} falls linearly from $I_M/2$ to 0, whereas i_{cb} rises from 0 to $I_M/2$ with the same rate so as to ensure the continuous dc current I_M. Similarly, the latter carries out commutation through both u_{diffa} and u_{diffb}, where $u_{diffa}=U_H/2n-U_{diff}$ and $u_{diffb}=U_H/2n+U_{diff}$. Hence, the arm inductor and the transformer leakage inductor of phase a share the U_{diff}, whereas phase b is opposite. As a result, i_a falls and i_b rises linearly to maintain continuous dc current I_H. Meanwhile, the voltage of u_{comc} and u_{diffc} should be kept as $U_M/2$ and $U_H/2n$ respectively, so that i_{ca} and i_c is not affected within the commutation time T_c. Due to symmetry of waveforms, the analysis of the other stages is not repeated here.

Through above analysis, MMC-DCT repeats the holding stage and the commutation stage in coordination with three-phase arms to maintain stable operation. Considering only the charging process of SM capacitor in each operation cycle, the capacitor voltage ripple ΔU_c for MMC-DCT can be obtained:

$$\Delta U_C=\frac{(1+m)}{2m}(1-m)\times\frac{P}{6NU_C C_{SM} f_h} \quad (3)$$

where m, the modulation ratio, is equal to the ration of $U_H/2n$ and $U_M/2$; P is the transferred power of MMC-DCT; U_C and C_{SM} are the rated voltage and capacitance of SM capacitor, respectively; f_h is the operation frequency. According to Eq. (3), the capacitor voltage ripple can be decreased to nearly zero at the high m because of the reshaped circulating current.

3 Parameter Design

The parameters of MMC-DCT mainly contain the number of SMs per arm N and passive components. Firstly, the sum voltage of all SM capacitors within one arm should be higher than the maximum arm voltage. Hence, the number of SMs required for each arm can be given as:

$$N\geq\frac{U_H}{2nU_C}+\frac{U_M}{2U_C}+\frac{U_{com}-U_{diff}}{U_C} \quad (4)$$

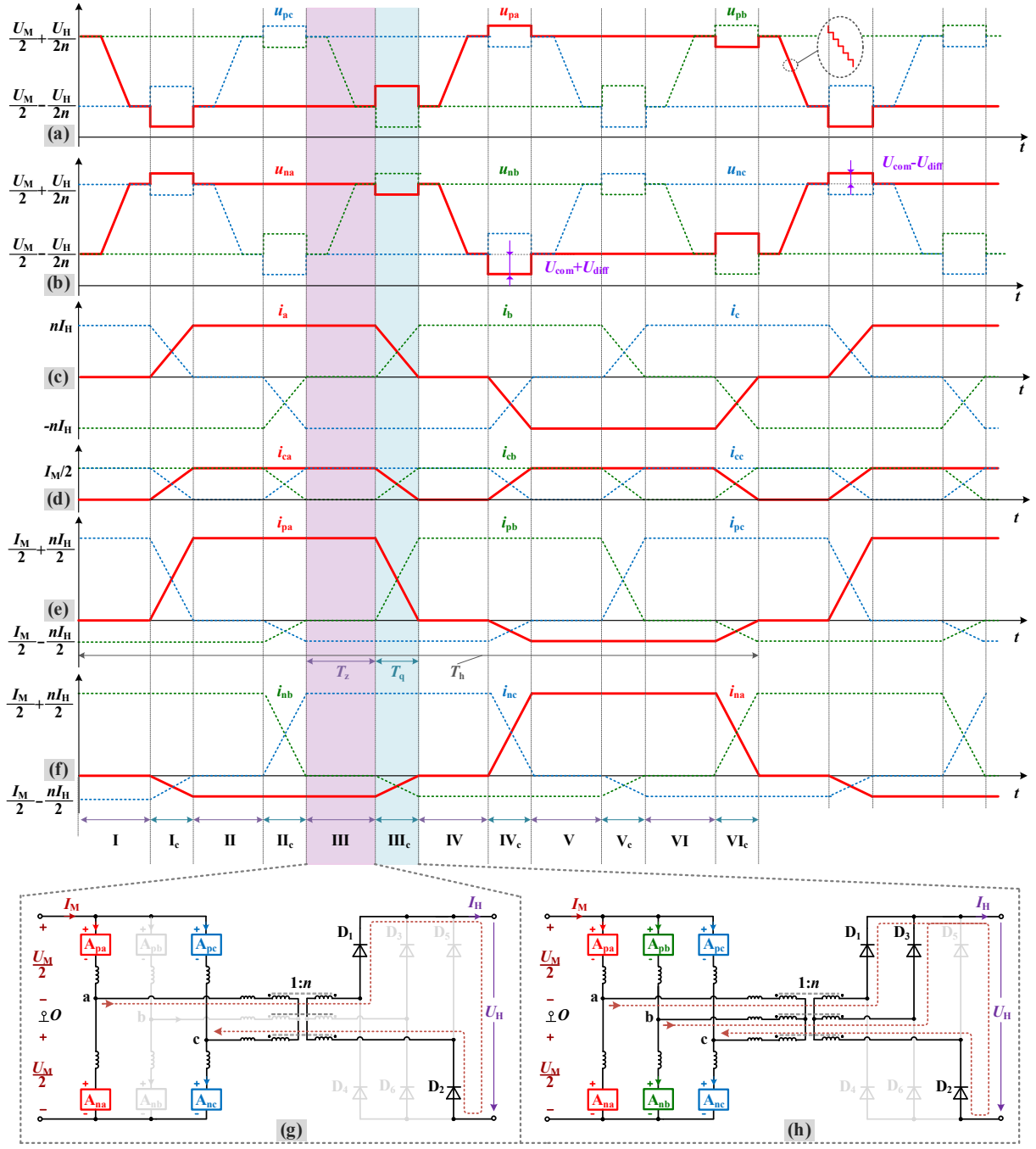

Fig. 2. Principle waveforms of the MMC-DCT. (a) Upper arm voltages. (b) Lower arm voltages. (c) Transformer currents. (d) Circulating currents. (e) Upper arm currents. (f) Lower arm currents. (g) Equivalent circuit corresponding to stage III. (h) Equivalent circuit corresponding to stage III$_c$.

where U_C is determined based on the voltage level of power devices; U_{com} and U_{diff} are usually designed as the 5%~10% U_M. Besides, each SM capacitor is typically designed to tolerate the allowable voltage ripple $\Delta U_{C,max}$. According to Eq. (3), the SM capacitance C_{SM} can be derived:

$$C_{SM} \geq \frac{(1+m)}{2m}(1-m)\times\frac{P}{6NU_C\Delta U_{C,max}f_h} \tag{5}$$

The design of arm inductance L and transformer leakage inductance L_k needs to take both commutation voltage U_{com}, U_{diff} and dc current ripple into consideration. The higher inductance results in higher U_{com}, U_{diff}, while the lower inductance results in higher dc current ripple. Hence, the range of inductance is:

$$\begin{cases} L\leq\dfrac{2U_{com}T_c}{I_M} & \dfrac{L}{2}+L_k\leq\dfrac{U_{diff}T_c}{nI_H} \\ L\geq\dfrac{3U_C}{4\varepsilon_i I_M f_s} & L_k\geq\dfrac{3U_C}{4\varepsilon_i nI_H f_s} \end{cases} \tag{6}$$

where ε_i is the relative dc current ripple; f_s is the SM switching frequency.

4 Simulation and Experimental Results

A simulation of 50MW MMC-DCT converting 50kV to 400kV is built and emulated in Matlab/Simulink. There are 30 SMs per arm and the rated capacitor voltage is 1.67kV. The operation frequency f_h is 150 Hz. More detailed simulation parameters are shown in Table 1.

Table 1 Simulation parameters

Parameters	Simulation
Rated power P	50MW
MVDC voltage U_M	50kV
HVDC voltage U_H	400kV
SM number per arm N	30
SM capacitance C_{SM}	3.25mF
SM capacitor voltage U_c	1.67kV
Transformer ratio n	10
Leakage inductance L_k	0.5mH
Arm inductance L	1mH
Commutation time T_c	0.56ms
Operation frequency f_h	150Hz

Fig. 3. shows the steady-state simulation waveforms of MMC-DCT where u_{c1}~u_{c6} are the average SM capacitor voltage within each arm, respectively. As shown in Fig.3.(a), the dc currents at both MVDC and HVDC side are smooth, with the value of 1kA (I_M) and 1.25kA (I_H), respectively. During the holding stage III, only two phases at MVDC side are in on-state. The circulating currents shown in Fig.3.(b) and transformer currents shown in Fig.3.(c) keep constant where i_{ca}=i_{cc}=500A (I_M/2) and i_a=-i_c=1250A (nI_H). Besides, as shown in Fig.3.(d) and (e), the SMs within phase b are switched with ZCS due to i_{pb}=i_{nb}=0 and du/dt stress is limited during u_{pb} and u_{nb} ramping down and up process depicted in Fig.3.(f) and (g). For the commutation stage III$_c$, phase a and phase b commutate linearly and phase c holds as constant, where the commutation voltage U_{com} and U_{diff} are designed as 0.9kV and 2.25kV respectively. As shown in Fig.3.(h), the average SM capacitor voltage within each arm are well balanced at 1.67kV (U_C). The relevant capacitor voltage ripple is kept as 77.4V, which is coincident with the theoretical analysis based on Eq. (3).

As shown in Fig. 4, a downscaled MMC-DCT prototype rated at 200V/400V, 2kW is bulit and tested to further verify effectiveness of the abovementioned analysis. The prototype includes power circuit with its main controller using a TMS320F28377D DSP plus two EP3C25Q240, EP3C10E144C8N FPGA. There are six SMs per arm and the selected SM capacitor is

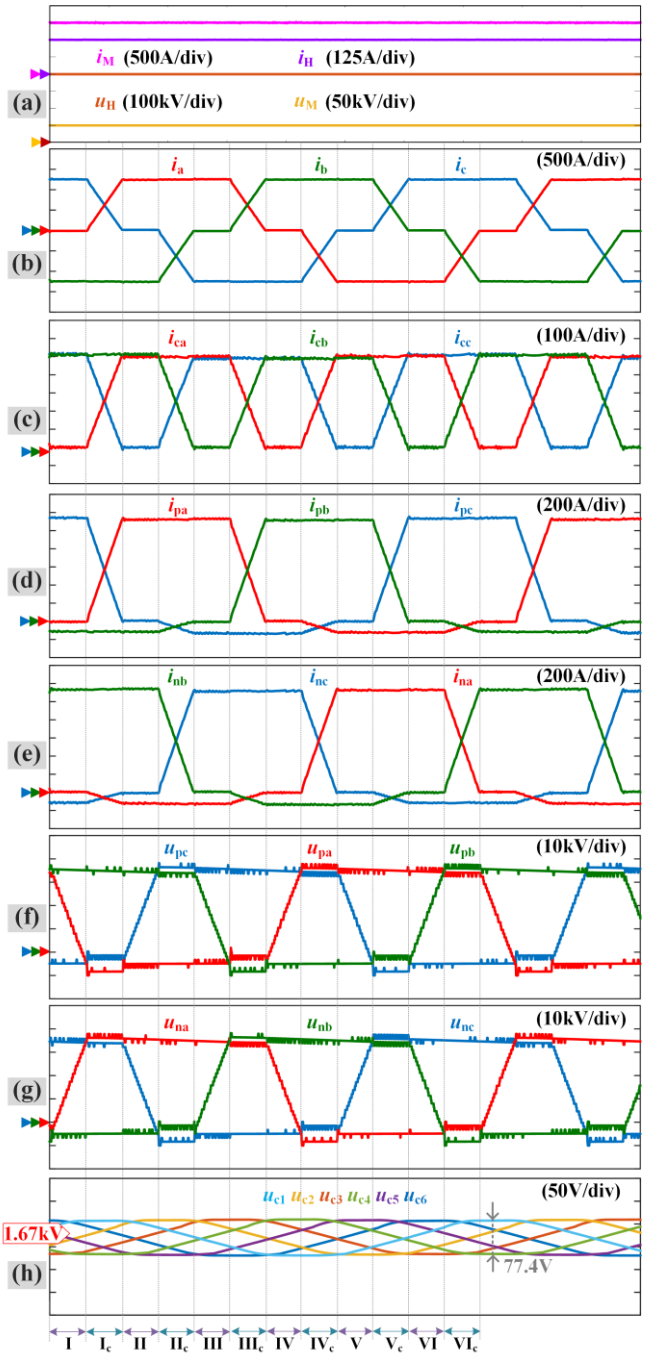

Fig. 3. Simulation results of the MMC-DCT: (a) Currents and voltages of two dc sides. (b) Transformer currents. (c) Circulating currents. (d) Upper arm currents. (e) Lower arm currents. (f) Upper arm voltages. (g) Lower arm voltages. (h) SM capacitor voltages of reshaped circulating current.

composed of three LGG2G102MELC50 electrolytic capacitors (0.1mF) in parallel to enhance its current tolerance. The 1KW30N60T (600V) IGBTs are employed in the SMs of MVDC side, whereas the DD100N16S diodes (1600V) are adopted forming the rectifier bridge of HVDC side. Three single-phase transformers with n=3 are used in Y-Y connections. More experimental parameters are listed in Table II. Experimental results as depicted in Fig.5 is consistent

Table 2 Experimental parameters

Parameters	Experiment
Rated power P	2kW
VDC voltage U_M	200V
HVDC voltage U_H	400V
SM number per arm N	6
SM capacitance C_{SM}	0.3mF
SM capacitor voltage U_c	33.3V
Transformer ratio n	3
Leakage inductance L_k	0.1mH
Arm inductance L	1mH
Commutation time T_c	0.75ms
Operation frequency f_h	150Hz

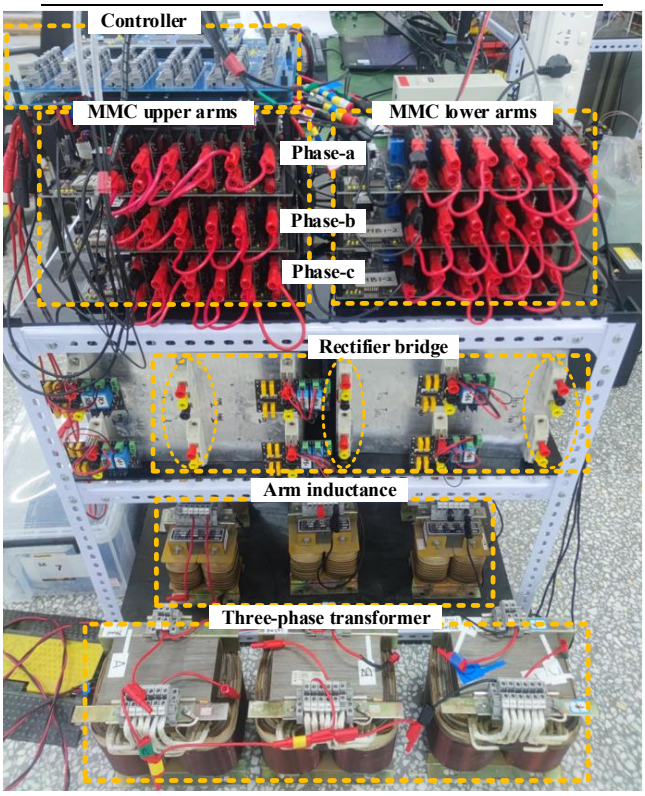

Fig. 4. Experimental prototype.

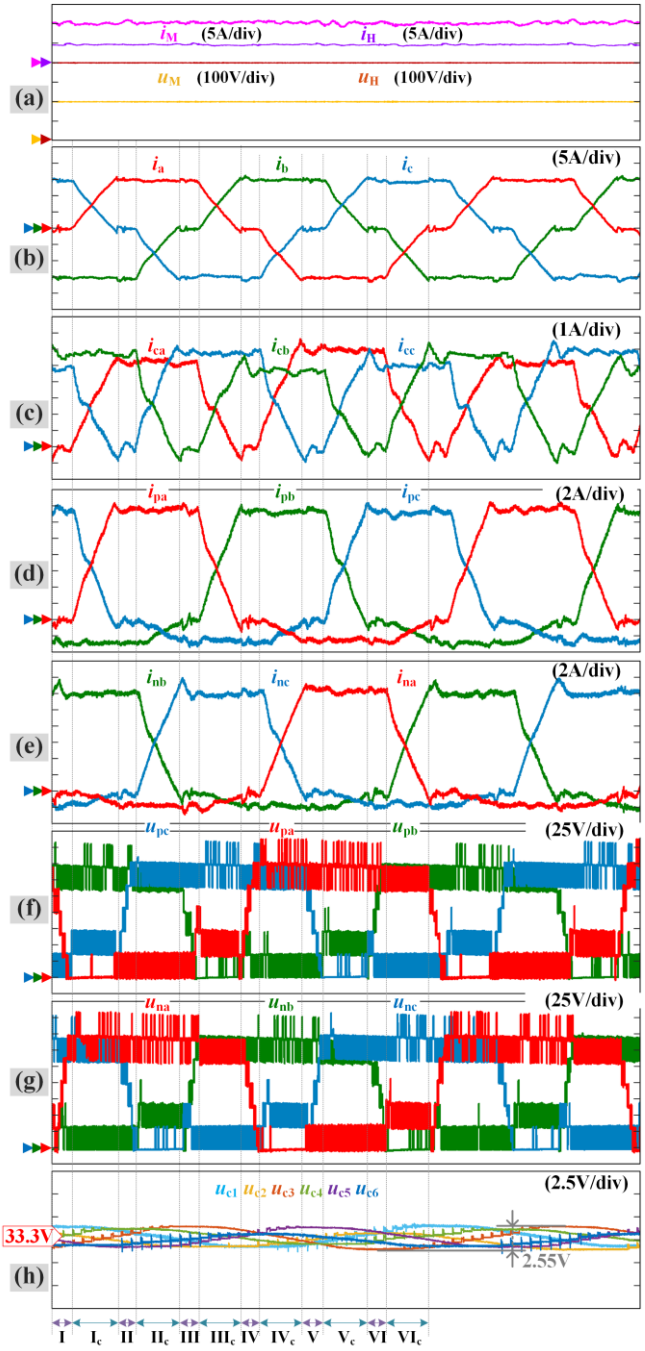

Fig. 5. Experimental results of the MMC-DCT: (a) Currents and voltages of two dc sides. (b) Transformer currents. (c) Circulating currents. (d) Upper arm currents. (e) Lower arm currents. (f) Upper arm voltages. (g) Lower arm voltages. (h) SM capacitor voltages of reshaped circulating current.

with simulation results. However, due to the limited number of SMs per arm, the arm voltage disturbance caused by SMs switching can not be neglected. Hence, the currents shown from Fig.5.(a) to (e) are not ideal waves, which exist some switching-frequency harmonics. In addition, as shown in Fig.5.(c), there are certain visible fluctuations in three-phase circulating currents due to the effect of energy balance between the upper and lower arms.

5 Discussions

The circulating current mainly affects SM capacitor voltage ripple, which determines the SM capacitance as well as the cost and volume of whole converter system. The conventional circulating current is usually designed as dc wave with the amplitude of $I_M/3$. The corresponding SM capacitor voltage ripple can be derived as:

$$\Delta U_C = \frac{(1+m)}{2m}\left(1-\frac{2m}{3}\right)\left(1-2m\frac{T_c}{T_h}\right)\times\frac{P}{6NU_C C_{SM} f_h} \quad (7)$$

Hence, according to Eq. (3) and (7), comparison between two type circulating currents regarding the voltage ripple normalized to $P/(6NU_CC_{SM}f_h)$ is shown in Fig. 6, where the commutation time T_c is selected as 0.56 ms same as the simulation. As can be seen, the voltage ripple of reshaped circulating current is much lower than that of conventional dc circulating current, especially when the modulation ratio m is higher than 0.8, it can be reduced by at least 50%. Therefore, it confirmed that the reshaped circulating current can significantly suppress the SM capacitor voltage ripple compared to the conventional dc circulating current.

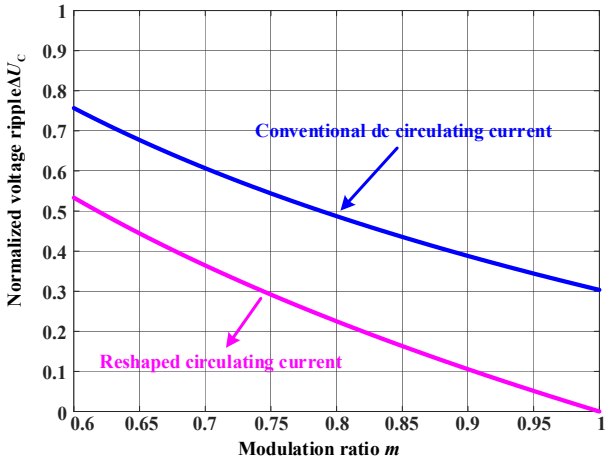

Fig. 6. Comparsion of normalized voltage ripple between conventional dc circulating current and reshaped circulating current.

6 Conclusions

In this paper, the MMC-DCT with reshaped circulating current is presented for the dc offshore wind farms, which aims to achieve MVDC collection and HVDC transmission. Smooth dc currents can be obtained in the arrangement of three-phase arms without any extra filters. Compared with the conventional dc circulating current, the SM capacitor voltage ripple can be decreased to nearly zero at the high modulation ratio and the switching loss of power devices within SMs can be reduced as well. Simulation and experimental results verify the effectiveness of the proposed reshaped circulating current strategy.

7 Acknowledgements

This work was supported by the National Natural Science Foundation of China under Grant 52177173 and “Fundamental Research Funds for the Central Universities” (Grant No.HIT.OCEF.2022009)

8 References

[1] J. A. Ferreira, "The Multilevel Modular DC Converter," in IEEE Transactions on Power Electronics, vol. 28, no. 10, pp. 4460-4465, Oct. 2013.

[2] G. J. Kish, M. Ranjram and P. W. Lehn, "A Modular Multilevel DC/DC Converter With Fault Blocking Capability for HVDC Interconnects," in IEEE Transactions on Power Electronics, vol. 30, no. 1, pp. 148-162, Jan. 2015.

[3] S. Kenzelmann, A. Rufer, D. Dujic, F. Canales and Y. R. de Novaes, "Isolated DC/DC Structure Based on Modular Multilevel Converter," in IEEE Transactions on Power Electronics, vol. 30, no. 1, pp. 89-98, Jan. 2015.

[4] G. Lambert, M. V. Soares, P. Wheeler, M. L. Heldwein and Y. R. de Novaes, "Current-Fed Multipulse Rectifier Approach for Unidirectional HVDC and MVDC Applications," in IEEE Transactions on Power Electronics, vol. 34, no. 4, pp. 3081-3090, April 2019.

[5] L. Guo, Y. Liu, L. Xu, F. Wang, L. Bao and H. Li, "Square-Wave Modulation for High-frequency Modular Multilevel DC-DC Converter with High Voltage-Conversion Ratio," 2022 9th International Forum on Electrical Engineering and Automation (IFEEA), Zhuhai, China, 2022, pp. 62-75.

[6] J. Yang, Z. He, H. Pang and G. Tang, "The Hybrid-Cascaded DC–DC Converters Suitable for HVdc Applications," in IEEE Transactions on Power Electronics, vol. 30, no. 10, pp. 5358-5363, Oct. 2015.

[7] S. Cui, N. Soltau and R. W. De Doncker, "A High Step-Up Ratio Soft-Switching DC–DC Converter for Interconnection of MVDC and HVDC Grids," in IEEE Transactions on Power Electronics, vol. 33, no. 4, pp. 2986-3001, April 2018.